First-Principles Phonon Quasiparticle Theory Applied to a Strongly Anharmonic Halide Perovskite

Terumasa Tadano[*]

Research Center for Magnetic and Spintronic Materials, National Institute for Materials Science,
Tsukuba 305-0047, Japan

Wissam A. Saidi

National Energy Technology Laboratory, United States Department of Energy,
Pittsburgh, Pennsylvania 15236, USA
and Department of Mechanical Engineering and Materials Science (MEMS), University of Pittsburgh,
Pittsburgh, Pennsylvania 15261, USA

Understanding and predicting lattice dynamics in strongly anharmonic crystals is one of the long-standing challenges in condensed matter physics. Here, we propose a first-principles method that gives accurate quasiparticle (QP) peaks of the phonon spectrum with strong anharmonic broadening. On top of the conventional first-order self-consistent phonon (SC1) dynamical matrix, the proposed method incorporates frequency renormalization effects by the bubble self-energy within the QP approximation. We apply the developed methodology to the strongly anharmonic α-CsPbBr$_3$ that displays phonon instability within the harmonic approximation in the whole Brillouin zone. While the SC1 theory significantly underestimates the cubic-to-tetragonal phase transition temperature (T_c) by more than 50%, we show that our approach yields $T_c = 404$–423 K, in excellent agreement with the experimental value of 403 K. We also demonstrate that an accurate determination of QP peaks is paramount for quantitative prediction and elucidation of the phonon linewidth.

Lattice vibrations in functional materials often exhibit strong anharmonicity; i.e., thermal or quantum fluctuation of atoms is so large that lattice dynamics cannot be predicted accurately by the quasiharmonic phonon theory. Notable examples of such materials include perovskites [1–3], thermoelectric materials [4–6], and superconducting hydrides [7,8]. In particular, halide perovskites have been attracting growing interest due to their unique physical properties, including high photovoltaic performance [9] along with relevant electron-phonon coupled physics and ultralow thermal conductivity [3,10]. However, an in-depth theoretical understanding and quantitative predictions of the lattice dynamics and phonon-related properties in these materials are still challenging due to the lack of first-principles computational approaches that can describe with high fidelity the intricate complexities associated with anharmonic behavior. In principle, lattice anharmonicity can be fully captured using *ab initio* molecular dynamics based on density functional theory (DFT). However, this approach is of limited use, because it invariably requires the use of large supercells to capture phonon-phonon interactions involving nonzero-wave-vector phonons and a long simulation time to extract well-converged values of the band- and momentum-resolved phonon frequencies and

linewidths. Thus, such simulations can quickly develop into a computational bottleneck.

To mitigate these challenges, several quasiparticle (QP)-like approaches have been proposed in the past decade [11–15]. Although QP approximation cannot describe satellite peaks, i.e., incoherent parts of spectra, it has several advantages. Namely, it simplifies the evaluation of physical quantities such as group velocity and heat capacity, allowing for a direct comparison with experiment. Besides, the QP treatment gives an *effective* one-body Hamiltonian of interacting phonons that is necessary as input for calculations of electron-phonon and phonon-phonon couplings in functional materials. The first-order self-consistent phonon (SC1) theory is one of the most successful methods, which determines the renormalized phonon frequencies by the variational principle applied to the first-order cumulant expansion of the Helmholtz free energy [16,17]. Since the SC1 theory can, to a large extent, remedy the negative frequency problems of the harmonic approximation, it has been actively employed in first-principles calculations of phonon-related physics of anharmonic materials, including thermal transport [13,18–21], phonon-limited mobility [22], band-gap renormalization [23,24], thermal expansion [25,26], and conventional

superconductivity [7,12,27]. While these studies clearly demonstrate the advantage of the SC1 theory over the quasiharmonic theory and purely perturbative approaches, the quantitative accuracy of SC1 is still inadequate for strongly anharmonic materials. More specifically, SC1 theory tends to overpredict phonon frequencies at finite temperatures, because it neglects the frequency shift associated with the bubble self-energy. Indeed, as we will show below, such a shift is substantial in the strongly anharmonic CsPbBr$_3$ and has significant effects on the theoretical phase transition temperature and phonon linewidth.

In this Letter, we propose a first-principles phonon calculation method that gives accurate QP peaks of a phonon spectrum broadened by phonon-phonon interactions. The developed method, which we formulate using the modern language employed in the GW approximation in electronic structure theory [28], incorporates the frequency shift by the bubble self-energy within the QP approximation and thereby solves the overestimation problem inherent to the SC1 theory. We apply the developed method to cubic CsPbBr$_3$ (α phase), which displays strong lattice anharmonicity accompanying the cubic-to-tetragonal phase transition at $T_c = 403$ K [29]. Although the SC1 theory underpredicts T_c by more than 50%, the QP theory gives T_c values of 404–423 K, which successfully reproduce the experimental value. We also show that the lattice thermal conductivity (LTC) of α-CsPbBr$_3$ calculated based on the QP theory combined with a beyond-Boltzmann treatment [30] is ultralow (< 0.5 W/mK at 500 K) and shows weak temperature dependence, whereas the LTC based on SC1 shows a clear trend of overestimation, thus highlighting the importance of an accurate determination of QP peaks for quantitative prediction of the phonon linewidth and LTC.

Reliable modeling of lattice dynamics requires an accurate treatment of lattice anharmonicity, which is manifested as an interaction between noninteracting (harmonic) phonons. This problem can be formulated by the Dyson equation as

$$\{G_q(\omega)\}^{-1} = \{G_q^0(\omega)\}^{-1} - \Sigma_q[G](\omega), \quad (1)$$

where $G_{qij'}^0(\omega)$ is the noninteracting phonon propagator and $\Sigma_q[G](\omega)$ is the anharmonic self-energy. For the self-energy, the most important terms associated with the third- and fourth-order anharmonicity are usually considered as $\Sigma_q[G](\omega) = \Sigma_q^T[G, \Phi_3] + \Sigma_q^L[G, \Phi_4] + \Sigma_q^B[G, \Phi_3](\omega)$. Here, T, L, and B stand for the tadpole, loop, and bubble diagrams, respectively. Their dependence on anharmonic force constants (Φ_3, Φ_4) is indicated explicitly. Once the above Dyson equation is solved for $G(\omega)$, the information of lattice dynamics can be obtained from the spectral function $A_q(\omega) = |\mathrm{Im}G_q(\omega)|/\pi$. However, achieving a fully self-consistent solution to Eq. (1) is challenging, because both sides of the equation depend on G and ω.

The SC1 theory greatly simplifies Eq. (1) as

$$\{G_q^S(\omega)\}^{-1} = \{G_q^0(\omega)\}^{-1} - \Sigma_q^T[G^S, \Phi_3] - \Sigma_q^L[G^S, \Phi_4], \quad (2)$$

where the ω-dependent $\Sigma_q^B[G, \Phi_3](\omega)$ is dropped. While the SC1 theory is powerful in its versatility and reasonable accuracy, the frequency shift associated with the neglected bubble diagram is not small [8,17] and particularly large in α-CsPbBr$_3$, as we will show below. Hence, $\Sigma_q^B[G, \Phi_3](\omega)$ should be included. Given that the SC1 propagator $G_q^S(\omega)$ is reasonably close to the fully dressed propagator $G_q(\omega)$, we may simplify Eq. (1) as

$$\{G_q(\omega)\}^{-1} \approx \{G_q^S(\omega)\}^{-1} - \Sigma_q^B[G^S, \Phi_3](\omega), \quad (3)$$

where the self-consistency for G is lifted. This is similar to the G_0W_0 approximation in electronic structure, where the Kohn-Sham wave function is used for the noninteracting part and the correlation is treated in "one shot" with $\Sigma = iG_0W_0$. So far, Eq. (3) has been employed to calculate the phonon spectral function of anharmonic solids [17,31]. However, instead of calculating the ω-dependent propagator, we aim to develop an *effective* one-body Hamiltonian that well represents the QP peaks given by Eq. (3). To this end, we propose the following self-consistent equation [32]:

$$\Omega_{q\nu}^2 = (\omega_{q\nu}^S)^2 - 2\omega_{q\nu}^S \mathrm{Re}\Sigma_{q\nu}^B[G^S, \Phi_3](\omega = \Omega_{q\nu}). \quad (4)$$

Here, $\omega_{q\nu}^S$ is the SC1 frequency, and the bubble self-energy is evaluated at the QP frequency $\Omega_{q\nu}$. The above nonlinear equation, again resembling the QP approximation in the GW calculations [28], needs to be solved self-consistently for $\Omega_{q\nu}$. To simplify this, it is tempting to linearize $\Sigma_{q\nu}^B[G^S, \Phi_3](\Omega_{q\nu})$ around $\Omega_{q\nu} = \omega_{q\nu}^S$, yielding $\Omega_{q\nu}^2 = (\omega_{q\nu}^S)^2 - 2Z_{q\nu}\omega_{q\nu}^S \mathrm{Re}\Sigma_{q\nu}^B[G^S, \Phi_3](\omega_{q\nu}^S)$ with $Z_{q\nu} = [1 + (\partial \mathrm{Re}\Sigma_{q\nu}^B/\partial\omega)|_{\omega=\omega_{q\nu}^S}]^{-1}$ being the renormalization factor. However, we found that this linearization yields a non-smooth temperature dependence of $\Omega_{q\nu}$ due to the complex ω dependence of $\mathrm{Re}\Sigma_{q\nu}^B(\omega)$. Hence, we do not employ such linearization in this study. Instead of the nonlinear QP equation [Eq. (4)], which we call QPNL, several different QP treatments are possible. The simplest is the static approximation ($\omega = 0$), which incorporates the first-order correction term that appears in the Hessian of the SC1 free energy [33]. Another option is to set $\omega = \omega_{q\nu}^S$. For the clarity of the following discussion, we denote these QP methods as QP[0] and QP[S], respectively. QP[S] is equivalent to setting $Z_{q\nu} = 1$ in the above linearized equation. We note that, beyond this one-shot treatment of the bubble self-energy would be possible with an approximation akin to that used in the QP self-consistent GW method [34], which is left for a future study.

We now apply the developed QPNL method to α-CsPbBr$_3$. The DFT calculations were conducted using

QUANTUM ESPRESSO [35], with the GGA-PBEsol functional [36]. The lattice dynamics calculations were performed using ALAMODE [37]. To include thermal expansion effects, we evaluated $F_{\text{vib}}^{(S)}(V, T)$ at various volumes and temperatures. The T-dependent volume was then obtained by minimizing the Helmholtz free energy as $V^{(S)}(T) = \arg\min_V\{E_0(V) + F_{\text{vib}}^{(S)}(V, T)\}$. This approach was shown to work even for the cases where the quasiharmonic theory breaks down due to the presence of unstable modes [25]. Harmonic and anharmonic interatomic force constants necessary for the lattice dynamics calculations were estimated using a compressed sensing approach [38] based on adaptive LASSO [39]. More details are provided in Supplemental Material [40].

We first discuss the T-dependent lattice constant shown in Fig. 1(b). The optimized value obtained by DFT is 5.868 Å that agrees exceptionally well with the experimental value of 5.873 Å at 473 K [48]. However, this almost perfect agreement is accidental as inferred after accounting for phonon excitations. Namely, at the SC1 level, we obtained 5.941 Å at 480 K that overestimates the experimental value by ~1%. The calculated linear thermal expansion coefficient of $\alpha \simeq 25 \times 10^{-6}$ K^{-1} is consistent with experimental results 28–33 $\times 10^{-6}$ K^{-1} [49].

In α-CsPbBr$_3$, phonon softening occurs in the whole Brillouin zone, as can be inferred at the harmonic level [Fig. 1(a)]. After accounting for anharmonic effects, these soft modes became dynamically stable in the high-temperature region, and their frequencies decrease gradually with cooling following the Curie-Weiss law, as we elaborate below. The calculated temperature dependence of these soft modes are shown in Figs. 1(c) and 1(d). The SC1 theory always yields stable phonons when the self-consistent equation [Eq. (2)] converges. Notwithstanding, we can estimate T_c by fitting the linear part of $(\omega_{q\nu}^S)^2$ with $A(T - T_c)$; see Table I. Given that the cubic-to-tetragonal phase transition is first order [29] with a small temperature hysteresis of ~7 K [50], the prediction based on the Curie-Weiss law should be interpreted as a lower bound of T_c. As seen from the table, SC1 significantly overestimates the soft mode frequencies and thereby underestimates T_c, which is less than 50% of the experimental T_c of 403 K.

Including the bubble diagram by solving Eq. (4), we can see from Fig. 1(c) and Table I that the T_c value is in better agreement with experiment. The QPNL method with $V = V_0$ gives a T_c value of 404–423 K, which agrees reasonably well with the experimental value. Also, the static QP[0] theory led to T_c values that are similar to those of the QPNL method. This is reasonable, because the QP energy approaches zero ($\Omega_{q\nu} \to 0$) in the limit of $T \to T_c$; hence, $\Sigma_{q\nu}^B(\Omega_{q\nu})$ approaches $\Sigma_{q\nu}^B(0)$. By contrast, the QP[S] frequencies were generally larger than that of the static approximation, and the T_c value became lower by ~40 K. All of these results clearly highlight the significant effect of

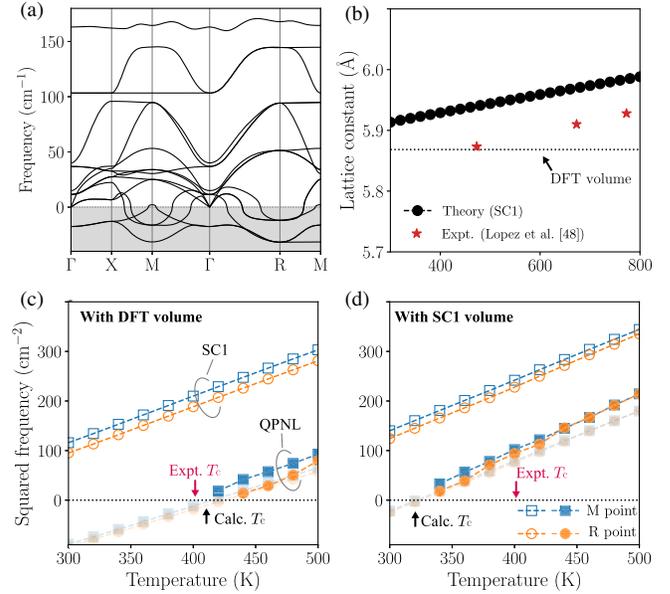FIG. 1. Calculated phonon frequency and lattice constant of α-CsPbBr$_3$. (a) Harmonic phonon dispersion calculated with $V = V_0$. (b) Temperature dependence of $V^{(S)}(T)$ compared with the experimental data [48]. (c) and (d) Temperature dependence of the squared frequency of soft modes at M and R points with $V = V_0$ and $V = V^{(S)}(T)$. The QP[0] results are shown by translucent symbols.

the bubble diagram. Moreover, we observed that the T_c value is quite sensitive to the lattice constant. When we used the SC1 volume, the frequencies of the soft modes at M and R points became larger than those obtained with the DFT volume, which can be attributed to their negative Grüneisen parameters [40]. Consequently, the estimated T_c value decreases by ~20% even though the difference in the lattice constant is only ~1% (see Sec. S3 in Supplemental Material [40]). Since a DFT lattice constant depends on the choice of the exchange-correlation functional and pseudopotential, the present result indicates the importance of carefully choosing them in the quantitative predictions of T_c for CsPbBr$_3$. A similar sensitivity has also been reported for BaTiO$_3$ [51].

To obtain insight into the accuracy of the QP theory over a wider frequency range, the calculated anharmonic phonon

TABLE I. Critical temperature (K) of the cubic-to-tetragonal phase transition calculated at different levels of the QP theory. The two values in each cell show the T_c values estimated from the soft mode frequency at M and R points, respectively. The experimental T_c is 403 K [29].

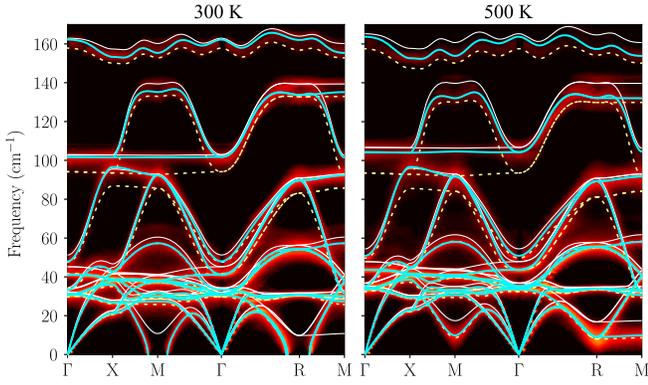| Method	DFT volume	SC1 volume
SC1 [Eq. (2)]	177, 198	164, 183
QP[0]	415, 424	322, 324
QP[S]	369, 382	303, 307
QPNL [Eq. (4)]	404, 423	319, 324

FIG. 2. Anharmonic phonon dispersion curves and spectral function of cubic CsPbBr$_3$ calculated (a) below and (b) above $T_c = 403$ K. The white thin lines, yellow dashed lines, and cyan solid thick lines represent the dispersion curves obtained within the SC1 theory, QP[0] theory, and the QPNL theory, respectively. The color map shows the spectral function $A_q(\omega)$. The volume is set to $V = V_0$.

FIG. 3. Lattice thermal conductivity and phonon lifetimes in α-CsPbBr$_3$ calculated using different dynamical matrices as inputs. (a) Lattice thermal conductivity κ_L [Eq. (5)] above the theoretical T_c values. (b) Phonon lifetimes $\tau_{q\nu} = \hbar/2\Gamma_{q\nu}^{3ph}$ at 500 K. (c) Spectral decomposition of the Peierls term calculated at 500 K. All calculations are done with $V = V_S(T)$.

dispersion curves are compared with the spectral function in Fig. 2. Here, the spectral function $A_q(\omega)$ is obtained from $G_q(\omega)$ of Eq. (3) with full frequency dependence of $\Sigma_{q\nu}^B(\omega)$ and is used as a reference to assess the accuracy of the QP theory. The SC1 theory tends to overestimate the phonon frequency as compared to the peak frequency of $A_q(\omega)$. The overestimation is particularly notable in the low-frequency soft modes that are still stable below T_c (left panel). Such overestimation is mostly rectified by the QP theory, irrespective of the adopted value for ω. However, Fig. 2 clearly shows that QP[0] underestimates the phonon frequencies above ~ 70 cm^{-1} as compared to $A_q(\omega)$. The underestimation of the optical modes around 100 cm^{-1} is as large as 10 cm^{-1}. We found that the QPNL theory is free from such an under- or overestimation artifact and thereby best represents the peak frequency of $A_q(\omega)$ (solid lines in Fig. 2). Therefore, we posit that QPNL gives the most reliable *effective* one-particle picture among the investigated approximations. We also found that the QP[S] gives similar results to QPNL although slightly overestimates the frequencies in the low-frequency region at low temperatures (see Fig. S3 in Supplemental Material [40]). Although more comprehensive study is needed, we expect the bubble frequency correction affects the soft-mode frequencies and associated physical properties, such as T_c and dielectric permittivity, in a broad range of materials that exhibit structural phase transition.

The strong modifications of the phonon band structures due to anharmonic effects uncovered by the QP theories beyond SC1 is expected to have a strong influence on the phonon linewidth. To uncover such effects, we calculated the phonon linewidths as $\Gamma_{q\nu}^{3ph} = \text{Im}\Sigma_{q\nu}^B[G, \Phi_3](\Omega_q)$. As shown in Fig. 3(b), the difference in the input dynamical matrix results in notable change in the phonon lifetime (inverse linewidth); the lifetime becomes the longest
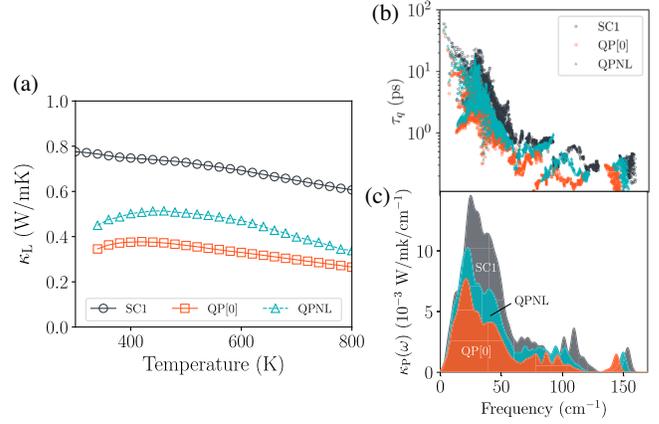
(shortest) with the SC1 (QP[0]) frequency. When the phonon frequency is overestimated, the scattering phase space will be underestimated because of a smaller occupation number $n_{q\nu} = [\exp(\beta\hbar\omega_{q\nu}) - 1]^{-1}$. Besides, the strength of the three-phonon interaction will be smaller due to the weaker hybridization [52]. These combined effects explain the factor of 2 difference in $\tau_{q\nu}$; with the SC1 frequency, the average phonon lifetime below 50 cm^{-1} is ~ 6.2 ps at 500 K, whereas it becomes ~ 2.7 ps with the QP [0] frequency.

We compared the calculated phonon frequency and linewidth with the experimental values [53] for the transverse acoustic modes along the $G - X$ and $G - M$ lines. As shown in Fig. S5 in Supplemental Material [40], the SC1 overestimates the TA phonon frequencies, while QP[0] and QPNL agree better with the experimental data. As for the linewidth, the calculated $\Gamma_{q\nu}^{3ph}$ was smaller than the experimental values even when the QPNL dynamical matrix was used, which indicates the potential role of higher-order phonon scattering processes. To examine this, we also computed the four-phonon scattering rate $\Gamma_{q\nu}^{4ph}$ following Refs. [54,55]. As shown in Fig. S5, the total linewidth $\Gamma_{q\nu} = \Gamma_{q\nu}^{3ph} + \Gamma_{q\nu}^{4ph}$ agrees reasonably well with the experimental values only when the QPNL dynamical matrix is used.

Next, we investigate the influence of the input dynamical matrix on LTC of α-CsPbBr$_3$. To this end, we evaluated the LTC using a two-channel model as [30]

$$\kappa_L = \frac{1}{N_q V} \sum_{q\nu\nu'} \frac{c_{q\nu}\omega_{q\nu'} + c_{q\nu'}\omega_{q\nu}}{\omega_{q\nu} + \omega_{q\nu'}} v_{q\nu\nu'} \otimes v_{q\nu'\nu}$$
$$\times \frac{\Gamma_{q\nu} + \Gamma_{q\nu'}}{(\omega_{q\nu} - \omega_{q\nu'})^2 + (\Gamma_{q\nu} + \Gamma_{q\nu'})^2}, \quad (5)$$

where $c_{q\nu}$ is the mode heat capacity, V is the unit-cell volume, and $v_{q\nu\nu'} = 1/2(\omega_{q\nu}\omega_{q\nu'})^{-1/2}\langle\eta_{q\nu}|\partial_q C(q)|\eta_{q\nu'}\rangle$ is the interband generalization of the group velocity [56] with $C(q)$ and $|\eta_{q\nu}\rangle$ being the dynamical matrix and polarization vector, respectively. The band diagonal term $(\nu = \nu')$ corresponds to the Peierls contribution (κ_P) within the relaxation-time approximation, whereas the off-diagonal term gives the coherent contribution (κ_C); the total LTC is given as $\kappa_L = \kappa_P + \kappa_C$. When calculating the phonon frequency and $v_{q\nu\nu'}$, we used the effective second-order force constants obtained from either the SC1 or QP eigenfrequencies and eigenvectors. Simoncelli, Marzari, and Mauri applied Eq. (5) to orthorhombic CsPbBr$_3$, combined with $\Gamma_{q\nu} \approx \Gamma_{q\nu}^{3ph}$, and obtained excellent agreements with experimental LTC [30]. Hence, we employ the same approximation for $\Gamma_{q\nu}$. Note that the inclusion of the four-phonon scattering process in Eq. (5) is technically straightforward, but it can underestimate LTC of strongly anharmonic materials because of the missing contributions from anharmonic heat flux [57].

Figure 3(a) shows the temperature-dependent κ_L calculated with three different dynamical matrices: SC1, QP[0], and QPNL. As seen in the figure, SC1 gives the largest κ_L, while QP[0] gives the smallest values. The difference mostly originated from κ_P, and κ_C was rather insensitive to the adopted dynamical matrix. The calculated phonon lifetimes and the spectra of the Peierls term $\kappa_P(\omega)$ are shown in Figs. 3(b) and 3(c), respectively. The $\kappa_P(\omega)$ data clearly show that κ_P is dominated by the low-frequency phonons below 50 cm^{-1}, and the difference among SC1, QP[0], and QPNL is most notable in this frequency region. From Fig. 2 (right panel), the phonon group velocity $v_{q\nu\nu}$ does not change appreciably in the three QP theories at 500 K. Indeed, the difference in κ_P can be attributed to the phonon lifetime. Consequently, a factor of 2 difference was observed also in κ_P: 0.68, 0.30, and 0.44 W/mK with the SC1, QP[0], and QPNL frequencies, respectively. Interestingly, we found that the phonon lifetimes $\tau_{q\nu} = \hbar/2\Gamma_{q\nu}^{3ph}$ of α-CsPbBr$_3$ are as large as those in $\alpha - \text{SrTiO}_3$ [17], whose LTC at 500 K is larger than 7 W/mK. Hence, the small group velocity also contributes to realizing ultralow LTC of α-CsPbBr$_3$, in accord with the previous interpretation [58].

For the coherent term κ_C, we obtained 0.051, 0.065, and 0.060 W/mK at 500 K using SC1, QP[0], and QPNL dynamical matrices, respectively; these values were nearly temperature independent above T_c. In comparison to the κ_C value of 0.3 W/mK (300 K) reported for the orthorhombic CsPbBr$_3$ [30], the coherent term for the cubic phase was smaller by a factor of ~5–6. This is reasonable considering that the number of phonon branches is 15 in the cubic phase, while it is 60 in the orthorhombic phase. Even for the cubic phase, the coherent term accounts for more than 13%

of the total LTC when the QP dynamical matrix is used and, therefore, should not be neglected.

The κ_L values at 500 K predicted by the SC1, QP[0], and QPNL theories are 0.73, 0.37, and 0.50 W/mK, respectively. Although no experimental κ_L value is available for α-CsPbBr$_3$, we expect it would be similar to that of the orthorhombic phase $\kappa_L \sim 0.4$ W/mK at 300 K [59]. More recently, $\kappa_L \sim 0.46$ W/mK at 500 K has been reported for another all-inorganic halide perovskite α-CsSnBr$_3$ [10]. Since the phonon frequencies of α-CsPbBr$_3$ and α-CsSnBr$_3$ are quantitatively similar, a similar κ_L value is expected for α-CsPbBr$_3$. Judging from these estimations, SC1 appears to overpredict the LTC of α-CsPbBr$_3$, and the predictions by the QP theories look more reasonable. We expect that calculations based on QPNL are the most reliable, at least theoretically, because it best represents the peak positions of $A_q(\omega)$. This expectation should be validated by a future experimental study.

Although the developed QPNL approach still has a limitation in describing lattice dynamics involving dynamical disorder, it offers an improved description of an effective one-body Hamiltonian of anharmonic systems and, thereby, paves the way to more reliable predictions of various phonon-related properties in functional materials.

*TADANO.Terumasa@nims.go.jp

[1] M. Kozina, M. Fechner, P. Marsik, T. v. Driel, J. M. Glownia, C. Bernhard, M. Radovic, D. Zhu, S. Bonetti, U. Staub, and M. C. Hoffmann, Terahertz-driven phonon upconversion in SrTiO$_3$, Nat. Phys. 15, 387 (2019).

[2] F. Knoop, T. A. R. Purcell, M. Scheffler, and C. Carbogno, Anharmonicity measure for materials, Phys. Rev. Mater. 4, 083809 (2020).

[3] M. A. Haque, S. Kee, D. R. Villalva, W. Ong, and D. Baran, Halide perovskites: Thermal transport and prospects for thermoelectricity, Adv. Sci. 7, 1903389 (2020).

[4] O. Delaire, J. Ma, K. Marty, A. F. May, M. A. McGuire, M.-H. Du, D. J. Singh, A. Podlesnyak, G. Ehlers, M. D. Lumsden, and B. C. Sales, Giant anharmonic phonon scattering in PbTe, Nat. Mater. 10, 614 (2011).

[5] C. W. Li, J. Hong, A. F. May, D. Bansal, S. Chi, T. Hong, G. Ehlers, and O. Delaire, Orbitally driven giant phonon anharmonicity in SnSe, Nat. Phys. 11, 1063 (2015).

[6] K. Suekuni, C. H. Lee, H. I. Tanaka, E. Nishibori, A. Nakamura, H. Kasai, H. Mori, H. Usui, M. Ochi, T. Hasegawa, M. Nakamura, S. Ohira-Kawamura, T. Kikuchi, K. Kaneko, H. Nishiate, K. Hashikuni, Y. Kosaka, K. Kuroki, and T. Takabatake, Retreat from Stress: Rattling in a Planar Coordination, Adv. Mater. 30, 1706230 (2018).

[7] I. Errea, M. Calandra, C. J. Pickard, J. Nelson, R. J. Needs, Y. Li, H. Liu, Y. Zhang, Y. Ma, and F. Mauri, High-Pressure Hydrogen Sulfide from First Principles: A Strongly

Anharmonic Phonon-Mediated Superconductor, Phys. Rev. Lett. **114**, 157004 (2015).

[8] I. Errea, F. Belli, L. Monacelli, A. Sanna, T. Koretsune, T. Tadano, R. Bianco, M. Calandra, R. Arita, F. Mauri, and J. A. Flores-Livas, Quantum crystal structure in the 250-kelvin superconducting lanthanum hydride, Nature (London) **578**, 66 (2020).

[9] J. Huang, Y. Yuan, Y. Shao, and Y. Yan, Understanding the physical properties of hybrid perovskites for photovoltaic applications, Nat. Rev. Mater. **2**, 17042 (2017).

[10] H. Xie, S. Hao, J. Bao, T. J. Slade, G. J. Snyder, C. Wolverton, and M. G. Kanatzidis, All-inorganic halide perovskites as potential thermoelectric materials: Dynamic cation off-centering induces ultralow thermal conductivity, J. Am. Chem. Soc. **142**, 9553 (2020).

[11] O. Hellman, I. A. Abrikosov, and S. I. Simak, Lattice dynamics of anharmonic solids from first principles, Phys. Rev. B **84**, 180301(R) (2011).

[12] I. Errea, M. Calandra, and F. Mauri, Anharmonic free energies and phonon dispersions from the stochastic self-consistent harmonic approximation: Application to platinum and palladium hydrides, Phys. Rev. B **89**, 064302 (2014).

[13] T. Tadano and S. Tsuneyuki, Self-consistent phonon calculations of lattice dynamical properties in cubic $SrTiO_3$ with first-principles anharmonic force constants, Phys. Rev. B **92**, 054301 (2015).

[14] A. van Roekeghem, J. Carrete, and N. Mingo, Anomalous thermal conductivity and suppression of negative thermal expansion in ScF_3, Phys. Rev. B **94**, 020303(R) (2016).

[15] N. K. Ravichandran and D. Broido, Unified first-principles theory of thermal properties of insulators, Phys. Rev. B **98**, 085205 (2018).

[16] M. L. Klein and G. K. Horton, The rise of self-consistent phonon theory, J. Low Temp. Phys. **9**, 151 (1972).

[17] T. Tadano and S. Tsuneyuki, First-principles lattice dynamics method for strongly anharmonic crystals, J. Phys. Soc. Jpn. **87**, 041015 (2018).

[18] J. S. Kang, H. Wu, M. Li, and Y. Hu, Intrinsic low thermal conductivity and phonon renormalization due to strong anharmonicity of single-crystal tin selenide, Nano Lett. **19**, 4941 (2019).

[19] Y. Xia, K. Pal, J. He, V. Ozoliņš, and C. Wolverton, Particlelike Phonon Propagation Dominates Ultralow Lattice Thermal Conductivity in Crystalline Tl_3VSe_4, Phys. Rev. Lett. **124**, 065901 (2020).

[20] Y. Xia, V. I. Hegde, K. Pal, X. Hua, D. Gaines, S. Patel, J. He, M. Aykol, and C. Wolverton, High-Throughput Study of Lattice Thermal Conductivity in Binary Rocksalt and Zinc Blende Compounds Including Higher-Order Anharmonicity, Phys. Rev. X **10**, 041029 (2020).

[21] S. Kawano, T. Tadano, and S. Iikubo, Effect of halogen ions on the low thermal conductivity of cesium halide perovskite, J. Phys. Chem. C **125**, 91 (2021).

[22] Y. Zhao, C. Lian, S. Zeng, Z. Dai, S. Meng, and J. Ni, Anomalous electronic and thermoelectric transport properties in cubic Rb_3AuO antiperovskite, Phys. Rev. B **102**, 094314 (2020).

[23] C. E. Patrick, K. W. Jacobsen, and K. S. Thygesen, Anharmonic stabilization and band gap renormalization in the perovskite $CsSnI_3$, Phys. Rev. B **92**, 201205(R) (2015).

[24] Y.-N. Wu, W. A. Saidi, J. K. Wuenschell, T. Tadano, P. Ohodnicki, B. Chorpening, and Y. Duan, Anharmonicity explains temperature renormalization effects of the band gap in $SrTiO_3$, J. Phys. Chem. Lett. **11**, 2518 (2020).

[25] Y. Oba, T. Tadano, R. Akashi, and S. Tsuneyuki, First-principles study of phonon anharmonicity and negative thermal expansion in ScF_3, Phys. Rev. Mater. **3**, 033601 (2019).

[26] C. Kwon, Y. Xia, F. Zhou, and B. Han, Dominant effect of anharmonicity on the equation of state and thermal conductivity of MgO under extreme conditions, Phys. Rev. B **102**, 184309 (2020).

[27] W. Sano, T. Koretsune, T. Tadano, R. Akashi, and R. Arita, Effect of Van Hove singularities on high-Tc superconductivity in H_3S, Phys. Rev. B **93**, 094525 (2016).

[28] R. Martin, L. Reining, and D. Ceperley, *Interacting Electrons: Theory and Computational Approaches* (Cambridge University Press, Cambridge, England, 2016).

[29] S. Hirotsu, J. Harada, M. Iizumi, and K. Gesi, Structural phase transitions in $CsPbBr_3$, J. Phys. Soc. Jpn. **37**, 1393 (1974).

[30] M. Simoncelli, N. Marzari, and F. Mauri, Unified theory of thermal transport in crystals and glasses, Nat. Phys. **15**, 809 (2019).

[31] U. Aseginolaza, R. Bianco, L. Monacelli, L. Paulatto, M. Calandra, F. Mauri, A. Bergara, and I. Errea, Phonon Collapse and Second-Order Phase Transition in Thermoelectric SnSe, Phys. Rev. Lett. **122**, 075901 (2019).

[32] Here, we neglect the off-diagonal components of the bubble self-energy, which are less significant than the diagonal terms. Extension of including the off-diagonal components is possible.

[33] R. Bianco, I. Errea, L. Paulatto, M. Calandra, and F. Mauri, Second-order structural phase transitions, free energy curvature, and temperature-dependent anharmonic phonons in the self-consistent harmonic approximation: Theory and stochastic implementation, Phys. Rev. B **96**, 014111 (2017).

[34] M. van Schilfgaarde, T. Kotani, and S. Faleev, Quasiparticle Self-Consistent GW Theory, Phys. Rev. Lett. **96**, 226402 (2006).

[35] P. Giannozzi et al., Advanced capabilities for materials modelling with QUANTUM ESPRESSO, J. Phys. Condens. Matter **29**, 465901 (2017).

[36] J. P. Perdew, A. Ruzsinszky, G. I. Csonka, O. A. Vydrov, G. E. Scuseria, L. A. Constantin, X. Zhou, and K. Burke, Restoring the Density-Gradient Expansion for Exchange in Solids and Surfaces, Phys. Rev. Lett. **100**, 136406 (2008).

[37] T. Tadano, Y. Gohda, and S. Tsuneyuki, Anharmonic force constants extracted from first-principles molecular dynamics: Applications to heat transfer simulations, J. Phys. Condens. Matter **26**, 225402 (2014).

[38] F. Zhou, W. Nielson, Y. Xia, and V. Ozoliņš, Lattice Anharmonicity and Thermal Conductivity from Compressive Sensing of First-Principles Calculations, Phys. Rev. Lett. **113**, 185501 (2014).

[39] H. Zou, The adaptive lasso and its oracle properties, J. Am. Stat. Assoc. **101,** 1418 (2006).

[40] See Supplemental Material at http://link.aps.org/supplemental/10.1103/PhysRevLett.129.185901 for the detailed computational procedures, the temperature-dependent phonon dispersion curves of α-CsPbBr$_3$ calculated by SC1, QP[0], QP[S], and QPNL, the lattice constant dependence of various anharmonic properties and T_c, and comparison of calculated and experimental linewidths of transverse acoustic phonons, which includes Refs. [41–47].

[41] G. Prandini, A. Marrazzo, I. E. Castelli, N. Mounet, and N. Marzari, Precision and efficiency in solid-state pseudopotential calculations, npj Comput. Mater. **4,** 72 (2018).

[42] S. Baroni, S. d. Gironcoli, A. D. Corso, and P. Giannozzi, Phonons and related crystal properties from density-functional perturbation theory, Rev. Mod. Phys. **73,** 515 (2001).

[43] T. Hastie, R. Tibshirani, and M. Wainwright, *Statistical Learning with Sparsity: The Lasso and Generalizations* (Chapman & Hall/CRC, London, 2015).

[44] E. Fransson, F. Eriksson, and P. Erhart, Efficient construction of linear models in materials modeling and applications to force constant expansions, npj Comput. Mater. **6,** 135 (2020).

[45] Y. Wang, J. J. Wang, W. Y. Wang, Z. G. Mei, S. L. Shang, L. Q. Chen, and Z. K. Liu, A mixed-space approach to first-principles calculations of phonon frequencies for polar materials, J. Phys. Condens. Matter **22,** 202201 (2010).

[46] X. Gonze and C. Lee, Dynamical matrices, Born effective charges, dielectric permittivity tensors, and interatomic force constants from density-functional perturbation theory, Phys. Rev. B **55,** 10355 (1997).

[47] W. Li, J. Carrete, N. A. Katcho, and N. Mingo, ShengBTE: A solver of the Boltzmann transport equation for phonons, Comput. Phys. Commun. **185,** 1747 (2014).

[48] C. A. López, C. Abia, M. C. Alvarez-Galván, B.-K. Hong, M. V. Martínez-Huerta, F. Serrano-Sánchez, F. Carrascoso, A. Castellanos-Gómez, M. T. Fernández-Díaz, and J. A. Alonso, Crystal structure features of CsPbBr$_3$ perovskite prepared by mechanochemical synthesis, ACS Omega **5,** 5931 (2020).

[49] M. Rodová, J. Brožek, K. Knížek, and K. Nitsch, Phase transitions in ternary caesium lead bromide, J. Therm. Anal. Calorim. **71,** 667 (2003).

[50] S. Svirskas, S. Balčiūnas, M. Šimėnas, G. Usevičius, M. Kinka, M. Velička, D. Kubicki, M. E. Castillo, A. Karabanov, V. V. Shvartsman, M. d. R. Soares, V. Šablinskas, A. N. Salak, D. C. Lupascu, and J. Banys, Phase transitions, screening and dielectric response of CsPbBr$_3$, J. Mater. Chem. A **8,** 14015 (2020).

[51] S. Ehsan, M. Arrigoni, G. K. H. Madsen, P. Blaha, and A. Tröster, First-principles self-consistent phonon approach to the study of the vibrational properties and structural phase transition of BaTiO$_3$, Phys. Rev. B **103,** 094108 (2021).

[52] T. Tadano and S. Tsuneyuki, Quartic Anharmonicity of Rattlers and Its Effect on Lattice Thermal Conductivity of Clathrates from First Principles, Phys. Rev. Lett. **120,** 105901 (2018).

[53] M. Songvilay, N. Giles-Donovan, M. Bari, Z.-G. Ye, J. L. Minns, M. A. Green, G. Xu, P. M. Gehring, K. Schmalzl, W. D. Ratcliff, C. M. Brown, D. Chernyshov, W. Beek, S. Cochran, and C. Stock, Common acoustic phonon lifetimes in inorganic and hybrid lead halide perovskites, Phys. Rev. Mater. **3,** 093602 (2019).

[54] R. S. Tripathi and K. N. Pathak, Self-energy of phonons in an anharmonic crystal to O(δ^4), Il Nuovo Cimento B **21,** 289 (1974).

[55] T. Feng, L. Lindsay, and X. Ruan, Four-phonon scattering significantly reduces intrinsic thermal conductivity of solids, Phys. Rev. B **96,** 161201 (2017).

[56] P. B. Allen and J. L. Feldman, Thermal conductivity of disordered harmonic solids, Phys. Rev. B **48,** 12581 (1993).

[57] T. Sun and P. B. Allen, Lattice thermal conductivity: Computations and theory of the high-temperature breakdown of the phonon-gas model, Phys. Rev. B **82,** 224305 (2010).

[58] G. A. Elbaz, W.-L. Ong, E. A. Doud, P. Kim, D. W. Paley, X. Roy, and J. A. Malen, Phonon speed, not scattering, differentiates thermal transport in lead halide perovskites, Nano Lett. **17,** 5734 (2017).

[59] W. Lee, H. Li, A. B. Wong, D. Zhang, M. Lai, Y. Yu, Q. Kong, E. Lin, J. J. Urban, J. C. Grossman, and P. Yang, Ultralow thermal conductivity in all-inorganic halide perovskites, Proc. Natl. Acad. Sci. U.S.A. **114,** 8693 (2017).